Published in final edited form as:
Sens Actuators B Chem. 2016 February ; 223: 927–935. doi:10.1016/j.snb.2015.09.157.

Screen-printed electrode produced by printed-circuit board technology. Application to Cancer Biomarker Detection by means of plastic antibody as sensing material

Felismina T.C. Moreira[1], **M. Judite M.S. Ferreira**[2], **José R.T. Puga**[2], and **M. Goreti F. Sales**[1]

[1]BioMark-CINTESIS/ISEP, School of Engineering, Polytechnic Institute of Porto, Portugal

[2]TID-CINTESIS/ School of Engineering, Polytechnic Institute of Porto, Portugal

Abstract

This research work presents, for the first time, a screen-printed electrode (SPE) made on a PCB board with silver tracks (Ag) and a three electrode configuration (AgxO-working, AgxO-counter and Ag/AgxO-reference electrodes), following the same approach as printed-circuit boards (PCBs). This low cost and disposable device was tested for screening a cancer biomarker in point-of-care. The selected biomarker was carcinogenic embryonic antigen (CEA) protein, routinely used to follow-up the progression of specific cancer diseases.

The biosensor was constructed by assembling a plastic antibody on the Ag-working electrode area, acting as the biorecognition element of the device. The protein molecules that were entrapped on the polymer and positioned at the outer surface of the polypyrrole (PPy) film were removed by protease action. The imprinting effect was tested by preparing non-imprinted (NPPy) material, including only PPy as biorecognition element. Infrared and Raman studies confirmed the surface modification of these electrodes. The ability of the sensing material to rebind CEA was measured by several electrochemical techniques: cyclic voltammetry (CV), impedance spectroscopy (EIS) and square wave voltammetry (SWV). The linear response ranged from 0.05 to 1.25 *pg/mL* against logarithm concentration.

Overall, producing screen-printed electrodes by means of conventional PCB technology showed promising features, mostly regarding cost and prompt availability. The plastic antibody-based biosensor also seems to be a promising tool for screening CEA in point-of-care, with low response time, low cost, good sensitivity and high stability.

Keywords

Screen-printed electrodes; Printed circuit board; Molecular Imprinting; Electropolymerization; Carcinogenic embryonic antigen; Biosensor

*To whom correspondence should be addressed. BioMark, Sensor Research, Instituto Superior de Engenharia do Porto, R. Dr. António Bernardino de Almeida, 431, 4200-072 Porto, Portugal. goreti.sales@gmail.com; mgf@isep.ipp.pt. Tel: +351 228 340 544; Fax: +351 228 321 159.

Europe PMC Funders Author Manuscripts

Europe PMC Funders Author Manuscripts

1 Introduction

Screen-printed electrodes (SPEs) are emerging as (bio)sensing portable tools for on-site and point-of-care detection [1]. Such tools are made of a chemically inert and non-conductive substrate, over which screen-printing technology is applied to produce the necessary electrodes. In these, three electrodes are usually involved: working, reference and auxiliary. In this regard, electrochemically-based approaches are becoming of increasing interest, for providing compact and portable reading systems of fast response [2].

In practice, the portability of SPEs is a result of combining three electrodes in the same support and using compact transducing apparatus, as those employed in blood glucose monitoring. So far, there are several supports that have been used to assemble SPEs by screen-printing technology.

Plastic-based supports are the ones employed more often [3, 4]. An alternative material could be the conventional printed circuit board (PCB) support, widely employed in electronics, of low cost and easy fabrication. This simple and well established approach is presented herein as a simple and low cost method of producing SPEs. Silver conductive tracks are selected for this purpose due to their high conductivity.

In addition to the support, the sensing material at the working electrode should grant sensitive and stable responses. In this regard, biomimetic materials are currently emerging, as an alternative to natural antibodies, offering high stability and easy preparation. The most common way to produce such artificial receptors makes use of molecular imprinting technology. In this, the target molecule is entrapped in a polymeric matrix and subsequently removed, thereby generating artificial binding positions of complementary stereospatial arrangement. When the target biomolecule is a protein, such biomimetic materials are named plastic antibodies, because they interact with the biomolecule in a similar way to that of natural antibodies.

Thus, this work combines the novel PCB-based SPEs comprising Ag tracks with the use of an antibody-like biomimetic material as sensing element. This combination is applied herein to target a cancer biomarker. Cancer biomarkers are currently employed for early cancer detection, selection of a therapeutic approach, and follow-up of the disease progression in the course of chemotherapy [5, 6]. In all these applications, point-of-care analysis is mostly desired but not yet achieved. Present methods to screen cancer biomarkers in hospital facilities include enzyme-linked immunosorbent assay (ELISA) and chromatographic approaches [7], always established inside the analytical laboratory. Meanwhile, electrochemical biosensors are presently emerging in research context as possible alternative screening tools in cancer.

Carcinogenic embryonic antigen (CEA) is one of the biomarkers of clinical interest in cancer, currently employed to measure the course of the progression of colon rectal cancer (CRC) [8],[9]. CEA is an immunoglobulin glycoprotein of high molecular weight, with a glycosyl phosphatidylinositol modification that binds it into the cell membrane. It has an aberrant glycosylation profile, which is a common feature among many biomolecules circulating in the blood when cancer disease is present.

One may find several CEA biosensors reported in the literature where the sensing material is an antibody. Such devices make use of electrochemical [10–29], optical [30–34], radioimmunoassay [35–38], or mass [39–45] detection. Some biosensors also employ enzyme or aptamer (Shu et al. 2013) materials as sensing element, but as far as we know no work has been reported so far making use of a biomimetic material for CEA targeting.

Thus, the present work reports, for the first time, a SPE electrode with a three electrode system (Ag/working, Ag/counter and Ag/AgO reference) assembled by PCB technology. It was also combined with a novel biomimetic material as sensing element that was designed to target CEA, a cancer biomarker. The biomimetic material (assigned later as MPPy) consisted of an imprinted matrix of polypyrrole (PPy), assembled by electropolymerizing Py on the working electrode area, in the presence of CEA, followed by protein removal after proteolytic enzymatic activity. A non-imprinted (NPPy) film was prepared in parallel to assess the contribution of the imprinted sites to the overall analytical response. The analytical performance and application feasibility of the resulting device were evaluated by different electrochemical techniques, namely CV, EIS and SWV techniques.

2 Experimental section

2.1 Apparatus

All electrochemical data was collected in a potentiostat/galvanostat equipment from Metrohm Autolab, PGSTAT302N, equipped with a FRA module for EIS readings and controlled by Nova software. The Ag-SPEs were homemade by means of commercial PCB technology and making use of a conventional SPE configuration. In this, the working electrode was placed at the centre and in a circle format and surrounded by counter and reference electrodes (electrically separated from each other and allowing the counter to have a bigger surface area). SPE strip dimensions were 3.5 × 0.9 × 1.5 cm. The electrical circuits were all made in printed silver (working and counter electrodes made of silver, and reference electrode and electrical contacts made of silver). The SPEs were connected to a homemade switch box, allowing their direct interface with the potentiostat/galvanostat.

Direct analysis of the surface modifications made use a Fourier transform infrared spectroscopy (FTIR) equipment Nicolet iS10, Smart iTR, from Thermo Scientific, coupled to an attenuated total reflectance (ATR) accessory also from Thermo Scientific. Raman studies were made in a Thermo Scientific DXR Raman microscope system, including a 100 mW excitation laser of 532 *nm*.

2.2 Reagents and solutions

All chemicals employed in this work were of analytical grade. Aqueous solutions and washing was made with de-ionized or ultrapure Milli-Q water. CEA, proteinase K, Pyrrole (Py), and Phosphate buffered saline (PBS), Myoglobin (Myo), Creatinine (Crea), were obtained from Fluka; Hexaammineruthenium (III) chloride (Ru^{3+}) from Acros; and 4-(2-hydroxyethyl)-1-piperazineethanesulfonic acid (HEPES) buffer from Sigma.

Stock solutions of CEA (0.25 μg/mL) were prepared in PBS buffer, pH 7.2. Less concentrated standards were prepared by dilution of the previous one, making use of the

same buffer. Electrochemical evaluation of the modified surfaces was made in a 1.0×10^{-3} mol/L Ru^{3+} solution, also prepared in PBS, pH 7.2.

2.3 Electrode pre-treatment

Before use, the Ag-SPE electrode followed pre-treating procedures that consisted in oxidizing the reference, counter and work electrode to Ag_xO (Ag_2O and AgO) by means of an electrochemical technique. This was done by subjecting the SPE system to 20 CV consecutive cycles, between -0.5 and 0.5 *V*, in PBS buffer, at pH 8. The electrodes were ready for use after cleaning with ethanol and drying [46].

2.4 Assembling the sensing material

The imprinted material was assembled in two stages. The first one consisted of covering the three electrodes of the SPE with a solution of Py ($5.0x10^{-3}$ mol/L in PBS buffer) and CEA (0.10 μg/mL in PBS), and applying 15 CV cycles from -0.2 to 1.0 *V*, using a scan-rate of 50 mV/s. The resulting CEA/PPy film was visible to naked eye. At this stage, the working electrode format was Ag-SPE/CEA/PPy. In a second stage, the CEA film was washed with deionized water and incubated in proteinase K (500 μg/mL solution prepared in PBS buffer, pH 7.4), for 2 hours, in the dark. The resulting film (MPPy), Ag-SPE/–/PPy, was ready for use after washing several times in PBS buffer (to remove protein fragments and proteinase K), and rinsing with water MQ.

Non-imprinted sensing layers were assembled in parallel and making use of the same solutions. The overall procedure followed for this purpose was similar to the previous one, but using Py solutions instead of Py/CEA solutions. The resulting devices were named as NPPy and the final format Ag-SPE/PPy.

2.5 Qualitative characterization of the films

The chemical changes occurring at the working electrode surface were followed directly on the SPE working electrode without previous treatment. Films of MPPy (after CEA removal) and NPPy were analysed by FTIR and RAMAN spectroscopy.

FTIR was also conducted directly over the thin-film layer deposited after electropolymerization. The ATR accessory had a germanium-based support, offering full transparency over the wavenumber range 400–4000 cm^{-1} wavenumber. The number of scans was set to 150, and the resolution to 8.

Raman spectra were collected in the same position as the confocal microscopy images presented in Figure 1, by selecting a 5 mW laser power and 25 μm pinhole apertures. Signal-to-noise ratio (peak height/RMS noise) was set to a high value and fluorescence correction to a 5 order degree, following the Omnic software specifications.

2.6 Binding Isotherm studies

The binding kinetics of the adsorption of CEA to MPPy and NPPy films was measured by SWV and the data adjusted to the Langmuir isotherm model. This was done by applying equation 1, where I_S was the normalized current-density (in Acm^{-2}, accounting the blank

effect and the negative response), S the concentration of CEA (in mol/L) and I_{max} the maximum current density observed (in Acm^{-2}).

$$I_S = \frac{I_{\max}[S]}{K_D + [S]} \quad \text{(equation 1)}$$

This was done by incubating the sensing layer with CEA standards of increasing concentrations, ranging from 1.25 to 125pg/mL, and prepared in buffer. An incubation period of 15 minutes was set for each standard solution, followed by redox probe reading in SWV method. The collected data was employed to calculate the apparent dissociation constant (K_D) and maximum binding capacity (B_{max}). K_D indicated the protein concentration yielding half of the analytical maximum response [1, 47].

2.7 Electrochemical assays

All electrochemical measurements were conducted in triplicate and used as redox probe Ru (III) prepared in PBS buffer of pH 7.2. In CV assays the potentials were cycled from -0.8 to +0.8 V, at 50 mV/s scan-rate; and in SWV assays potentials changed from -0.8 to +0.8 V, at a frequency of 25 Hz and a step height of 150 mV. In general, EIS assays were made in triplicate with the Ru (III) redox couple, making use of an open circuit potential with a sinusoidal potential perturbation of 0.01 V amplitude and a number of frequencies equal to 50, over the 0.1–100 kHz frequency range.

The calibration curve procedure consisted of incubating increasing concentrations of standard CEA solutions, ranging from 1.25 pg/mL to 125 pg/mL, and prepared in PBS buffer, pH 7.2. The electrochemical data collected for this purpose included SWV and EIS measurements.

2.8 Selectivity study

The interfering species tested were selected among those that may be found in biological fluids, such as Myo (50 ng/mL) and Crea (0.01 mg/mL). This study was carried by its incubation during 15 minutes on (Ag-SPE/–/PPy) surface.

3 Results and discussion

3.1 Electrode pre-treatment

The electrical features of the novel SPEs were identified by recording several CV voltammograms of a suitable redox probe. While the peak to peak separation of the collected data was more or less as expected, repeated CV assays yielded significant changes in the absolute current values. This was attributed to changes at the silver surface of the electrodes generated by repeated electrical cycling modes, which eventually became visible to naked eye.

The stabilization of the current produced by the device was subsequently achieved by applying an oxidation procedure specifically to the silver reference electrode, yielding the

transformation of Ag into AgO nanoparticles. Such nanoparticles are expected to increase the electroactive area, thereby contributing to improve the analytical features of the biosensing device [46]. The specific procedure applied for this purpose followed a previously described approach [46, 48], after which all CV signals became stable and repeatable within time.

3.2 Design of the biomimetic sensing material

The selection of a suitable molecular-imprinting approach is essential to achieve a successful biomimetic recognition layer. In the specific case of protein targeting, where the biomolecule is a big sized nanostructure, mass transfer and protein removal from the imprinted polymer become fundamental requirements. These are met by surface imprinting, making this the most suitable approach for protein-imprinting. This approach is expected to lead to a high number of effective binding sites, thereby improving protein binding kinetics [49, 50].

In surface imprinting, the protein is bound to a receptor surface (in this study, the Ag working electrode) and a suitable polymer is grown around it. The polymerization stage must be established under close-to-physiological conditions to ensure that the imprinted biomolecule maintains its stereochemical arrangement (or close to it). This may be achieved by electropolymerization, where the desired chemical/physical proprieties of the polymeric film may be controlled by modulating several experimental parameters [50].

Among the several polymers produced by electropolymerization, PPy has been identified as a promising material for electrochemical transducing events, due to its excellent electrical properties, mostly related to high conductivity events [51–53]. Indeed, PPy electropolymerized films have been successfully produced by an oxidative process, achieved on the surface of noble metals such as platinum or gold [54, 55]. Some authors have used other non-noble metals, such as iron [56], zinc [57], copper [58] and iv), aluminum [59, 60], yielding chemical alterations at the receptor surface, depending of the specific electrochemical conditions employed.

In the specific work, where PPy films are to be assembled on a non-noble surface such as silver, the electrochemically formed film is expected to be arranged in a sandwich structure [61]. In this work, the PPy film is assembled in an oxide layer (AgxO) on the Ag-SPE surface, when electropolymerizing conditions are applied to an aqueous solution of Py. Such sandwich structure results from growing the polymer on a surface with a number of cracks, where the AgO layer is in fact heterogeneous. The confocal microscopy observation of the material evidenced such heterogeneous and cracked surface before PPy formation (Figure 1, left). Consequently, the initial electropolymerization of Py was preferentially established inside the cracks, thereby forming preferential conducting paths from the blank silver substrate to the outer surface of the growing AgO layer, consistent with the corresponding confocal microscopy images (Figure 1, right).

Overall, the imprinted MPPy films (Ag-SPE/–/PPy) were produced by polymerization of Py monomer that was initiated and sustained by electrical stimulus. The overall process was represented in Figure 2 and consisted on trapping CEA target biomolecules as the PPy thin-

film was being assembled at the receptor surface. The PPy film was formed by imposing several consecutive CV cycles to an aqueous solution of Py monomer containing CEA, from -0.2 to 0.8 *V* [62–65]. The final stage of the MPPy production consisted on removing the CEA biomolecules at the outer surface of the imprinted matrix by an enzyme. Enzymatic was preferred to chemical digestion in order to avoid chemical alterations at the outer layer of the polymeric surface. Proteinase K was the enzyme selected for this purpose because it displays high enzymatic activity with low cutting specificity.

The specific binding of CEA to the imprinted sites was assessed by comparing the response of the MPPy films to control films NPPy (Ag-SPE/PPy), assembled by the same procedure but without protein in the Py solution. While MPPy films may give rise to a combined response of specific and non-specific binding of CEA to the imprinted positions, the binding of CEA to NPPy films can only be established by means of non-specific interactions because no binding positions exist in these.

3.3 Follow-up of the biomimetic material assembly

The formation of the MPPy/NPPy films was evident to human eye, as the initial silver oxide electrode became black. This black color accounted the successful formation of the PPy film, regardless the presence of the protein. But the assembly of a biomimetic film was expected to promote alterations upon the electron transfer properties of the receptor surface, at the two main stages involved in the film assembly. Such electrical changes were followed herein by EIS and CV studies, providing consistent data as explained next.

The CV voltammogram of blank Ag-SPEs showed the reduction peak of Ru(III), reduced to Ru(II), but the corresponding current intensity was very low compared to that expected in the normal gold commercial SPEs (Figure 3A). The electropolymerization stage carried out next for assembling the MPPy films included several CV cycles that showed different current profiles.

The overall CV current increased in the 1st and 2nd cycle, but was followed by a decrease in the following cycles with subsequent stabilization up to the 15th cycle. Still, after PPy electropolymerization electrical improvements of the working electrode were observed. PPy is a conductive polymer and is considered as a pseudocapacitor. These materials show the capability to store charge *Faradically* through various charge transfer reactions between electrode and electrolyte, presenting high conductivity in charged state and low equivalent series resistance. The charge/discharge process in these types of pseudocapacitive materials is basically associated with the insertion/deinsertion of counter ions, arising from the electrolyte [66, 67].

The CV of the PPy sensory material showed higher current intensities and the reversibility of redox probe signal became more evident. This is due the formation of an eletroactive conductive film on Ag-SPE surface. The EIS data recorded for the Ag-SPE/CEA/PPy device was also consistent with the formation of a conductive layer that reflected the presence of the conductive polymer, PPy. Consistently, the Rct data of Ag-SPE/CEA/PPy films was lower than that of the original silver substrate (Figure 3B). In the next stage, the protein removal promotes a decrease in the overall CV current. This could be due to the partial

exposure of Ag_xO –SPE surface. This layer is less conductive than PPy, thereby leading to a resistance increase comparing with Ag-SPE/CEA/PPy sensor (with absence of cavities). When the sensor was incubated in CEA, the resistance increased due to the presence of protein biomolecules, most likely at their rebinding positions. Indeed, the protein (high molecular weight) was an additional barrier to the electron transfer over the polymer surface[67].

3.4 Qualitative analysis

The qualitative features of blank SPEs and biomimetic/control films were assessed by RAMAN analysis with confocal microscopy and FTIR studies directly on ATR support of Germanium crystal. The spectra of Ag-SPE, electrodes are shown in Figure 4.

The Raman spectra of Ag-SPE electrodes that followed electropolymerization evidenced the presence of carbon-based polymeric structures (as PPy). In these, the peak at ~1560 cm^{-1} (absent in Ag-SPE blank materials) was assigned to the presence of the Py aromatic rings [68]. Moreover, the changes in the double-peaks at 530–610 cm^{-1} confirmed the modifications made on the substrate, as these peaks were more intense on blank silver-based supports. The higher raman intensity at 2900 cm^{-1} in the spectra of Ag-SPE/CEA/PPy and Ag-SPE/PPy also evidenced the presence of functional groups out coming from the PPy matrix or the protein itself.

Comparing to Ag-SPE, the Ag-SPE/CEA/PPy and Ag-SPE/PPy FTIR spectra showed two well-defined and significant absorption peaks at ~1046 and 630 cm^{-1}, assigned to C–H/C–N stretching, and bending vibrations of C–H bonds in PPy [69, 70]. The presence of CEA in the material Ag-SPE/CEA/PPy was most probably related to the presence of a broad band centered at 3300 cm^{-1}. Such band could result from O–H/N–H stretches related to the several functional groups typically present in proteins.

Overall, both Raman and FTIR spectra showed significant differences between blank and modified Ag-SPEs. The data was consistent with the presence of a PPy polymeric film over the silver blank support. The presence of CEA within the PPy matrix was also supported by the presented data, mostly accounting the differences between Ag-SPE/CEA/PPy and Ag-SPE/PPy FTIR spectra.

3.5 Analytical performance of the sensor

The analytical features of Ag-SPE/—/PPy electrodes were checked by CV (Figure 5A), SWV (Figure 5B), and EIS (Figure 5C) measurements (Figure 5-1), and plotting subsequently the collected electrical data (Figure 5-2), expressed in current intensity (in SWV and CV) or R_{ct} (in EIS) against logarithm CEA concentration. The CEA concentrations selected for this purpose ranged from 1.25 to 125 *pg/mL*. Each standard concentration was allowed to bind to the sensing layer for a fixed period of 15 minutes.

In general, the presence of CEA on the surface decreased the background current provided by the electrode and such decrease was concentration dependent. CV data (Figure 5-A1) evidenced the redox peaks of the ruthenium probe, which decreased after the presence of CEA and in proportion to its concentration. EIS data, in the form of Nyquist plots, showed

increasing R_{ct} values as the concentration of CEA increased (Figure 5-C1). SWV data (Figure 5-B1) was again consistent with the previously mentioned behaviour, but this blocking effect was however linked to three peaks positioned at –0.20, +0.16 and +0.006 V. These peaks at –0.20, +0.006 and +0.16 V are from the anodic oxidation of silver. Anodic oxidation of silver is a complex reaction and the measurements depend strongly on the pre-treatment of the electrode surface. The main oxidation reactions are Ag, Ag- Ag_2O, Ag_2O-AgO[71, 72].

The first two anodic peaks are due to the electro-formation of AgOH and Ag_2O, respectively. The formation of AgOH occurred at the site on the silver surface, while the formation of Ag_2O takes place up to a limited depth within the crystallite silver. The peak at 0.16 V was associated with the completion the oxidation of Ag_2O to AgO at the outer/inner surface layer. Once, the formation of AgO initiated at the Ag_2O surface during the anodic scan, further formation of AgO becomes easier and occurs at a lower potential [71].

The typical calibration curves of Ag-SPE/—/PPy sensors obtained by CV, SWV and EIS assays are shown in Figure 5-2. The CV-based data obtained indicated a linear behaviour down to 1.25 pg/mL, with a slope -2.23 *μA/decade* log [CEA, *ng/mL*] and squared correlation coefficients > 0.98; the SWV data showed linear behaviour down to 1.25 *pg/mL*, but with a slope -0.231 *μA/decade* log [CEA, *ng/mL*] and squared correlation coefficients > 0.97; and EIS data also presented a linear response down to 1.25 pg/mL, with a slope average of 3.60 *KΩ/decade* log [CEA, *ng/mL*] and the squared correlation coefficients > 0.982.

The NPPy sensor responses were linked to a random behavior (in EIS) or to very low sensitivities (in CV and SWV), as shown in Figure 5-2. Such behavior indicated that the recognition of CEA was mostly governed by its binding to the imprinted sites, which suggested that the imprinting process was successfully established.

In general, more sensitive responses were achieved by CV measurements, but the other electrochemical approaches displayed similar linear concentration ranges of response. It can happens because PPy is a conductive polymer and is considered as a pseudocapacitor where the capacitance developed holds *Faradaic* origin, with process of chemical/electronic changes as formation/removal of radical cation or radical anion centers, indicating a pseudocapacitance character[66, 67].

In, cyclic voltammetry, the current that flows across the electrode-solution interface arises from two sources: i) *Faradaic* current which arises from the reduction or oxidation of the species in solution and ii) *Double layer* that forms at the electrode-solution interface, a significant capacitive current, which is called the n*on-Faradaic* current. The double layer is produced by the electrostatic attraction/repulsion of cations and anions respectively, near the electrode surface to balance the charge on the electrodes. In the side, square-wave voltammetry measurements are the combination of linear or staircase potential ramps with superimposed sequences of short potential pulses (10-50*mV* for 10-50 *ms*, discriminating against charging (capacitance) current [66, 67]. Capacitive contributions can be discriminated against, before they die away, since over a small potential range between

forward and reverse pulses, the capacity is constant and is thus annulled by subtraction. Pulse techniques are more sensitive to oxidation or reduction currents (*Faradaic currents*) than conventional DC voltammetry. Differential pulse voltammetry yields peaks for Faradaic excluding non-Faradaic currents [66, 67]. Thus, it is for this reason the sensitivity of the CV and SWV are different: in CV data, *no-Faradaic* are considered improving the overall net current.

Also, the response time of each electrical reading was always below 15 minutes and could be ranked as SWV < CV < EIS. All electrochemical techniques showed standard deviations below 5% for repeated measures. In general, both CV and SWV could be employed for practical analytical applications, but the selection of a specific one varies with which is more important: the intended sensitivity or the speed of response.

3.6 Binding Isotherm

Binding isotherm parameters may reveal relevant features regarding the adsorption of the target CEA to the imprinted sites or non-imprinted positions. As shown in previous work, the Langmuir model was found suitable for this purpose, [47] [1] llowing the calculation of binding capacity ($B_{máx}$) and dissociation constant (K_D) data. As in the Michaelis-Menton approach to enzymatic systems, such dissociation constant (K_D) indicated the necessary CEA concentration to get one half of the maximal velocity of the reaction. In general, a low K_D suggested a large binding affinity between CEA and its receptor surface, as the reaction would approach more rapidly its maximum signal; the maximum binding capacity (B_{max}) expressed the necessary CEA concentration to saturate all binding sites in the film (imprinted or non-imprinted positions). The experimental binding data was calculated by applying equation 1, where normalized current data was plotted against CEA concentration (Figure 6), and linearizing after the corresponding function to the Lineweaver-Burk plots.

This study compared the binding affinity data of Ag-SPE/—/PPy and Ag-SPE/PPy devices, aiming to identify in which extent the non-binding positions were contributing to the overall response of the electrodes. The obtained B_{max} and K_D values were 0.373 mA and 0.0058 *ng/mL* and 0.116 *mA* and 0.0090 *ng/mL*, respectively. In general, these results evidenced that Ag-SPE/—/PPy electrodes displayed higher binding affinity to CEA than Ag-SPE/PPy devices, thereby suggesting that the imprinted film had a high number of binding positions to which CEA should bind.

3.7 Reproducibility of the electrodes

The reproducibility of the molecularly imprinted modified Ag-SPE electrode was investigated for 0.025 *ng/mL* CEA. The peak current response of CEA was determined with 3 electrodes which produced under the same conditions. The response peak intensity showed a relative standard deviation of 8.2 % confirming that the results are reproducible.

3.8 Selectivity study

The selectivity was performed by incubation of the (Ag-SPE/–/PPy) biosensor with different interferents as Myo and Crea. The results are shown in the figure 7 and indicate low binding

of ability of Myo (8%) and Crea (2%) comparing with CEA (33%), meaning that the sensor have affinity for the target molecule.

3.9 Performance in spiked samples

Considering that measuring the selectivity of individual interfering species is far from the real conditions of application of any sensor, the selectivity of the device was further assessed by testing in real samples. For this purpose, the analytical performance of the biosensor was evaluated in real urine samples spiked with known amounts of CEA. The urine samples were obtained from healthy volunteer and diluted 10× to proceed with the calibration.

The calibration was made by successive addition starting from 1.25 pg/mL. A linear behavior was observed up to 125 pg/mL CEA, with a slope of -0.129 $\mu A/decade$ log [CEA, ng/mL]. The impact of real samples was observed on the slope only, rather than on the linear range. The existence of a linear tend in a well-defined region of CEA concentration, points out the possibility of using this new device in future testing of real samples.

4 Conclusions

PCB technology with Ag tracks has been shown to produce successful SPEs, offering great advantages in terms of cost. The real cost of each SPE gets down to the order of cents of euro, instead of a typical price of 3 to 7€ reported for similar commercial devices with different metals or carbon. Still, the use of Ag based SPE electrodes may offer limited stability due to environmental oxidation. Such limitation may be overcome by prior electrochemical pre-treatment stage, where the electrodes are oxidized and further stabilized.

In the present study, a novel biomimetic material for CEA cancer biomarker has been shown possible, yielding sensitive readings that were mostly governed by CEA binding to the imprinted sites. The extent of response sensitivity was dependent of the electrochemical approach, for which different techniques could and should be explored in order to maximize the potentialities of the SPE devices.

In general, the Ag-SPE based MPPy electrodes displayed short measuring time (with a maximum incubation period of 15 minutes), simple design (conventional PCB technology), precise readings (repeatable signals with a maximum of 5% change), and low limit of detection (in the order of pg CEA per mL). The novel combined approach proposed herein may lead to decreasing costs in SPE serial production, while offering sensing materials of high stability (when compared to the common natural antibodies used in immunosensing). The presented approach is expected to be further improved upon the application of different chemical pre-treating methods and/or surface modification procedures. This would open new horizons into the set-up of SPE disposable devices offering appropriate stability to be established in wide screening schemes of cancer biomarkers in point-of-care.

Acknowledgements

The authors acknowledge the financial support of European Research Council though the Starting Grant, ERC-StG-3P's/2012, GA 311086 (to MGF Sales).

References

[1]. Moreira FTC, Sharma S, Dutra RAF, Noronha JPC, Cass AEG, Sales MGF. Smart plastic antibody material (SPAM) tailored on disposable screen printed electrodes for protein recognition: Application to myoglobin detection. Biosens Bioelectron. 2013; 45:237–244. [PubMed: 23500370]

[2]. Hayat A, Marty JL. Disposable Screen Printed Electrochemical Sensors: Tools for Environmental Monitoring. Sensors. 2014; 14:10432–10453. [PubMed: 24932865]

[3]. Li M, Li Y-T, Li D-W, Long Y-T. Recent developments and applications of screen-printed electrodes in environmental assays-A review. Anal Chim Acta. 2012; 734:31–44. [PubMed: 22704470]

[4]. Niu X, Lan M, Zhao H, Chen C, Li Y, Zhu X. Review: electrochemical stripping analysis of trace heavy metals using screen-printed electrodes. Anal Lett. 2013; 46:2479–2502.

[5]. Basil CF, Zhao YD, Zavaglia K, Jin P, Panelli MC, Voiculescu S, Mandruzzato S, Lee HM, Seliger B, Freedman RS, Taylor PR, et al. Common cancer biomarkers. Cancer Res. 2006; 66:2953–2961. [PubMed: 16540643]

[6]. Tothill IE. Biosensors for cancer markers diagnosis. Semin Cell Develop Biol. 2009; 20:55–62.

[7]. Zhai X-H, Yu J-K, Yang F-Q, Zheng S. Identification of a new protein biomarker for colorectal cancer diagnosis. Mol Med Rep. 2012; 6:444–448. [PubMed: 22614045]

[8]. Soreide K, Nedrebo BS, Knapp J-C, Glomsaker TB, Soreide JA, Korner H. Evolving molecular classification by genomic and proteomic biomarkers in colorectal cancer: Potential implications for the surgical oncologist. Surg Onc Oxford. 2009; 18:31–50.

[9]. Tanaka T, Tanaka M, Tanaka T, Ishigamori R. Biomarkers for Colorectal Cancer. Int J Mol Sci. 2010; 11:3209–3225. [PubMed: 20957089]

[10]. Cai Y, Li H, Li Y, Zhao Y, Ma H, Zhu B, Xu C, Wei Q, Wu D, Du B. Electrochemical immunoassay for carcinoembryonic antigen based on signal amplification strategy of nanotubular mesoporous PdCu alloy. Biosens Bioelectron. 2012; 36:6–11. [PubMed: 22560438]

[11]. Cao X, Wang N, Jia S, Guo L, Li K. Bimetallic AuPt nanochains: Synthesis and their application in electrochemical immunosensor for the detection of carcinoembryonic antigen. Biosens Bioelectron. 2013; 39:226–230. [PubMed: 22921093]

[12]. Chen H, Tang D, Zhang B, Liu B, Cui Y, Chen G. Electrochemical immunosensor for carcinoembryonic antigen based on nanosilver-coated magnetic beads and gold-graphene nanolabels. Talanta. 2012; 91:95–102. [PubMed: 22365686]

[13]. Feng D, Lu X, Dong X, Ling Y, Zhang Y. Label-free electrochemical immunosensor for the carcinoembryonic antigen using a glassy carbon electrode modified with electrodeposited Prussian Blue, a graphene and carbon nanotube assembly and an antibody immobilized on gold nanoparticles. Microchim Acta. 2013; 180:767–774.

[14]. Feng D, Li L, Fang X, Han X, Zhang Y. Dual signal amplification of horseradish peroxidase functionalized nanocomposite as trace label for the electrochemical detection of carcinoembryonic antigen. Electrochim Acta. 2014; 127:334–341.

[15]. Gan N, Jia L, Zheng L. A Sandwich Electrochemical Immunosensor Using Magnetic DNA Nanoprobes for Carcinoembryonic Antigen. Int J Mol Sci. 2011; 12:7410–7423. [PubMed: 22174606]

[16]. Gao X, Zhang Y, Wu Q, Chen H, Chen Z, Lin X. One step electrochemically deposited nanocomposite film of chitosan-carbon nanotubes-gold nanoparticles for carcinoembryonic antigen immunosensor application. Talanta. 2011; 85:1980–1985. [PubMed: 21872047]

[17]. Han, J, Ma, Z. A Label-free Electrochemical Immunosensor for Carcinoembryonic Antigen Based on Graphene and ThionineAdvanced Research on Biochemical Materials and Nanotechnology Application. Zhang, H, Jin, D, Zhao, XJ, editors2013. 29–32.

[18]. Hu, N, Wang, P, Zhou, J, Du, L, Zou, L. Preparing electrochemical immunosensor, which is useful for detecting unmarked carcinoembryonic antigen, comprises carrying out magnetron sputtering on glass substrate using a titanium tungsten and gold film. Univ Zhejiang;

Europe PMC Funders Author Manuscripts

[19]. Huang K-J, Wu Z-W, Wu Y-Y, Liu Y-M. Electrochemical immunoassay of carcinoembryonic antigen based on TiO2-graphene/thionine/gold nanoparticles composite. Canadian J Chem-Revue Canad Chim. 2012; 90:608–615.

[20]. Li, Y, Zhang, Y, Wei, Q, Du, B, Li, H, Ma, H, Wu, D. Method for preparing alphafetoprotein and carcinoembryonic antigen electrochemical luminous immune sensor that is utilized for diagnosing liver cancer, involves preparing composite material and antibody marker, and forming gold film layer. Univ Jinan;

[21]. Lin D, Wu J, Ju H, Yan F. Nanogold/mesoporous carbon foam-mediated silver enhancement for graphene-enhanced electrochemical immunosensing of carcinoembryonic antigen. Biosens Bioelectron. 2014; 52:153–158. [PubMed: 24041661]

[22]. Miao J, Wang X, Lu L, Zhu P, Mao C, Zhao H, Song Y, Shen J. Electrochemical immunosensor based on hyperbranched structure for carcinoembryonic antigen detection. Biosens Bioelectron. 2014; 58:9–16. [PubMed: 24607616]

[23]. Pandey B, Demchenko AV, Stine KJ. Nanoporous gold as a solid support for protein immobilization and development of an electrochemical immunoassay for prostate specific antigen and carcinoembryonic antigen. Microchim Acta. 2012; 179:71–81.

[24]. Shu H, Wen W, Xiong H, Zhang X, Wang S. Novel electrochemical aptamer biosensor based on gold nanoparticles signal amplification for the detection of carcinoembryonic antigen. Electrochem Commun. 2013; 37:15–19.

[25]. Sun X, Ma Z. Highly stable electrochemical immunosensor for carcinoembryonic antigen. Biosens Bioelectron. 2012; 35:470–474. [PubMed: 22444512]

[26]. Sun X, Ma Z. Electrochemical immunosensor based on nanoporpus gold loading thionine for carcinoembryonic antigen. Anal Chim Acta. 2013; 780:95–100. [PubMed: 23680556]

[27]. Sun G, Lu J, Ge S, Song X, Yu J, Yan M, Huang J. Ultrasensitive electrochemical immunoassay for carcinoembryonic antigen based on three-dimensional macroporous gold nanoparticles/graphene composite platform and multienzyme functionalized nanoporous silver label. Anal Chim Acta. 2013; 775:85–92. [PubMed: 23601978]

[28]. Zhou J, Du L, Zou L, Zou Y, Hu N, Wang P. An ultrasensitive electrochemical immunosensor for carcinoembryonic antigen detection based on staphylococcal protein A-Au nanoparticle modified gold electrode. Sens Actuators, B. 2014; 197:220–227.

[29]. Zhu L, Xu L, Jia N, Huang B, Tan L, Yang S, Yao S. Electrochemical immunoassay for carcinoembryonic antigen using gold nanoparticle-graphene composite modified glassy carbon electrode. Talanta. 2013; 116:809–815. [PubMed: 24148478]

[30]. Denk H, Holzner JH, Tappeine G. Immunofluorescent optical detection of carcinoembryonic antigen in tumors of gastrointestinal tract. Wiener Klinische Wochenschrift. 1972; 84:400.

[31]. Huitric E, Burtin P, Laumonie R. Study on localization of carcinoembryonic antigen in cancerous and normal intestinal-mucosa in optical and electron-microscopy. Biol Gastro-Enterol. 1973; 6:363–363.

[32]. Huitric E, Laumonier R, Burtin P, Vonkleist S, Chavanel G. Optical and ultrastructural study of localization of carcinoembryonic antigen (cea) in normal and cancerous human rectocolonic mucosa. Lab Invest. 1976; 34:97–107. [PubMed: 1246127]

[33]. Matsuzawa S, Kimura H, Tu CY, Kitamori T, Sawada T. Quantitation of ige and carcinoembryonic antigen (cea) by optical beam deflection (obd) measurement of dot-immunobinding assay patterns visualized by an elisa technique. J Immunol Methods. 1993; 161:59–65. [PubMed: 7683704]

[34]. Venisnik KM, Olafsen T, Gambhir SS, Wu AM. Fusion of Gaussia luciferase to an engineered anti-carcinoembryonic antigen (CEA) antibody for in vivo optical imaging. J Imaging Biol. 2007; 9:267–277.

[35]. Tsaltas G, Ford CHJ, Gallant M. Demonstration of monoclonal anticarcinoembryonic antigen (cea) antibody internalization by electron-microscopy, western blotting and radioimmunoassay. Anticancer Res. 1992; 12:2133–2142. [PubMed: 1295459]

[36]. Kuroki M, Arakawa F, Higuchi H, Matsunaga A, Okamoto N, Takakura K, Matsuoka Y. Epitope mapping of the carcinoembryonic antigen by monoclonal-antibodies and establishment of a new improved radioimmunoassay system. J Cancer Res. 1987; 78:386–396.

[37]. Hetherington JW, Ewing R, Cooper EH. Evaluation of a double-monoclonal radioimmunoassay for the measurement of carcinoembryonic antigen in the urine of patients with bladder-cancer. Eur Urol. 1986; 12:270–273. [PubMed: 3743597]

[38]. Liu YSV, Tobias RJ, Zurawski VR. A more specific, simpler radioimmunoassay for carcinoembryonic antigen, with use of monoclonal-antibodies. Clin Chem. 1985; 31:191–195. [PubMed: 3967348]

[39]. Right-lower-quadrant mass and elevated serum carcinoembryonic antigen level. New York state journal of medicine. 1991; 91:394–398. [PubMed: 1945151]

[40]. Alpern HD, Olson JE, Hughes S, Stahl W, Bordley J. Right-lower-quadrant mass and elevated serum carcinoembryonic antigen level. New York State J Med. 1991; 91:394–398. [PubMed: 1945151]

[41]. Carroll PR, Pellegrini C, Hedgcock MW, Stein R, Williams RD. Microscopic hematuria, left renal mass with renal-vein obstruction and elevated serum level of carcinoembryonic antigen in a 56-year-old man. J Urol. 1983; 129:568–573. [PubMed: 6300473]

[42]. Chen B, Hu B, Jiang P, He M, Peng H, Zhang X. Nanoparticle labelling-based magnetic immunoassay on chip combined with electrothermal vaporization - inductively coupled plasma mass spectrometry for the determination of carcinoembryonic antigen in human serum. Analyst. 2011; 136:3934–3942. [PubMed: 21858374]

[43]. Li F, Shen Z, Lu Y, Wang L, Song W. How Much Does Body Mass Index Affect Serum Carcinoembryonic Antigen Concentration? Cancer Epidem Biomar. 2014; 23:555–560.

[44]. Shively JE, Hefta SA, Swiderek K, Wu A, Lee TD. Structural studies of carcinoembryonic antigen (CEA) and anti-CEA engineered antibodies using mass spectrometry. Protein Structure - Function Relationship. 1996:203–2012.

[45]. Xu, Y. Capturing carcinoembryonic antigen negative colorectal cancerproteome in biological samples useful for e.g. the kit of the protein fingerprint comprises utilizing magnetic bead, utilizing magnetic separator, and utilizing mass spectrometry, CN101241139-A.

[46]. Wang Y-H, Gu H-Y. Hemoglobin co-immobilized with silver-silver oxide nanoparticles on a bare silver electrode for hydrogen peroxide electroanalysis. Microchim Acta. 2009; 164:41–47.

[47]. Moreira FTC, Sharma S, Dutra RAF, Noronha JPC, Cass AEG, Sales MGF. Protein-responsive polymers for point-of-care detection of cardiac biomarker. Sens Actuators, B. 2014; 196:123–132.

[48]. Chiu M-H, Cheng W-L, Muthuraman G, Hsu C-T, Chung H-H, Zen J-M. A disposable screen-printed silver strip sensor for single drop analysis of halide in biological samples. Biosens Bioelectron. 2009; 24:3008–3013. [PubMed: 19342215]

[49]. Yildirim E, Turan E, Caykara T. Construction of myoglobin imprinted polymer films by grafting from silicon surface. J Mater Chem A. 2012; 22:636–642.

[50]. Moreira FTC, Dutra RAF, Noronha JPC, Sales MGF. Electrochemical biosensor based on biomimetic material for myoglobin detection. Electrochim Acta. 2013; 107:481–487.

[51]. Sadki S, Schottland P, Brodie N, Sabouraud G. The mechanisms of pyrrole electropolymerization. Chem Soc Rev. 2000; 29:283–293.

[52]. Truong LTN, Chikae M, Ukita Y, Takamura Y. Labelless impedance immunosensor based on polypyrrole-pyrolecarboxylic acid copolymer for hCG detection. Talanta. 2011; 85:2576–2580. [PubMed: 21962685]

[53]. Zhou M, Heinze J. Electropolymerization of pyrrole and electrochemical study of polypyrrole: 1. Evidence for structural diversity of polypyrrole. Electrochim Acta. 1999; 44:1733–1748.

[54]. Qu L, Xia S, Bian C, Sun J, Han J. A micro-potentiometric hemoglobin immunosensor based on electropolymerized polypyrrole-gold nanoparticles composite. Biosensors & Bioelectronics. 2009; 24:3419–3424. [PubMed: 19110412]

[55]. Errachid A, Caballero D, Crespo E, Bessueille F, Pla-Roca M, Mills CA, Teixidor F, Samitier J. Electropolymerization of nano-dimensioned polypyrrole micro-ring arrays on gold substrates prepared using submerged micro-contact printing. Nanotechnology. 2007; 18

[56]. Su WC, Iroh JO. Electrodeposition mechanism of polypyrrole coatings on steel substrates from aqueous oxalate solutions. Electrochim Acta. 2000; 46:1–8.

[57]. Batool A, Kanwal F, Imran M, Jamil T, Siddiqi SA. Synthesis of polypyrrole/zinc oxide composites and study of their structural, thermal and electrical properties. Synth Met. 2012; 161:2753–2758.

[58]. Fenelon AM, Breslin CB. The electrochemical synthesis of polypyrrole at a copper electrode: corrosion protection properties. Electrochem Acta. 2002; 47:4467–4476.

[59]. Turhan MC, Weiser M, Killian MS, Leitner B, Virtanen S. Electrochemical polymerization and characterization of polypyrrole on Mg-Al alloy (AZ91D). Synth Met. 2011; 161:360–364.

[60]. Liu AS, Oliveira MAS. Electrodeposition of polypyrrole films on aluminum from tartrate aqueous solution. J Braz Chem Soc. 2007; 18:143–152.

[61]. Ghadim, Morteza Farkhondekalam; F, G; Imani, Amin. Synthesis of PPy–silver nanocomposites via in situ oxidative polymerization. J Nanost Chem. 2014; 101:5.

[62]. Keothongkham K, Pimanpang S, Maiaugree W, Saekow S, Jarernboon W, Amornkitbamrung V. Electrochemically Deposited Polypyrrole for Dye-Sensitized Solar Cell Counter Electrodes. Int J Photoenergy. 2012:5305.

[63]. Hwang DK, Song D, Jeon SS, Han TH, Kang YS, Im SS. Ultrathin polypyrrole nanosheets doped with HCl as counter electrodes in dye-sensitized solar cells. J Mater Chem A. 2014; 2:859–865.

[64]. Veerender P, Saxena V, Jha P, Koiry SP, Gusain A, Samanta S, Chauhan AK, Aswal DK, Gupta SK. Free-standing polypyrrole films as substrate-free and Pt-free counter electrodes for quasi-solid dye-sensitized solar cells. Org Electron. 2012; 13:3032–3039.

[65]. Zhang X, Wang S, Lu S, Su J, He T. Influence of doping anions on structure and properties of electro-polymerized polypyrrole counter electrodes for use in dye-sensitized solar cells. J Power Sources. 2014; 246:491–498.

[66]. Sahoo S, Dhibar S, Das CK. Facile synthesis of polypyrrole nanofiber and its enhanced electrochemical performances in different electrolytes. Express Polymer Letters. 2012; 6:965–974.

[67]. Kujundziski AP, Chamovska D, Grchev T. Capacitive properties of polypyrrole/activated carbon composite. Hemijska Industrija. 2014; 68:709–719.

[68]. Li M, Wei Z, Jiang L. Polypyrrole nanofiber arrays synthesized by a biphasic electrochemical strategy. Journal of Materials Chemistry. 2008; 18:2276–2280.

[69]. Schmid A, Sutton LR, Armes SP, Bain PS, Manfre G. Synthesis and evaluation of polypyrrole-coated thermally-expandable microspheres: an improved approach to reversible adhesion. Soft Matter. 2009; 5:407–412.

[70]. Li CM, Sun CQ, Chen W, Pan L. Electrochemical thin film deposition of polypyrrole on different substrates. Surf Coat Tech. 2005; 198:474–477.

[71]. Droog JMM, Huisman F. Electrochemical formation and reduction of silver-oxides in alkaline media. J Electroanal Chem. 1980; 115:211–224.

[72]. Jovic BM, Jovic VD. Electrochemical formation and characterization of Ag2O. J Serbian Chem Soc. 2004; 69:153–166.

Europe PMC Funders Author Manuscripts

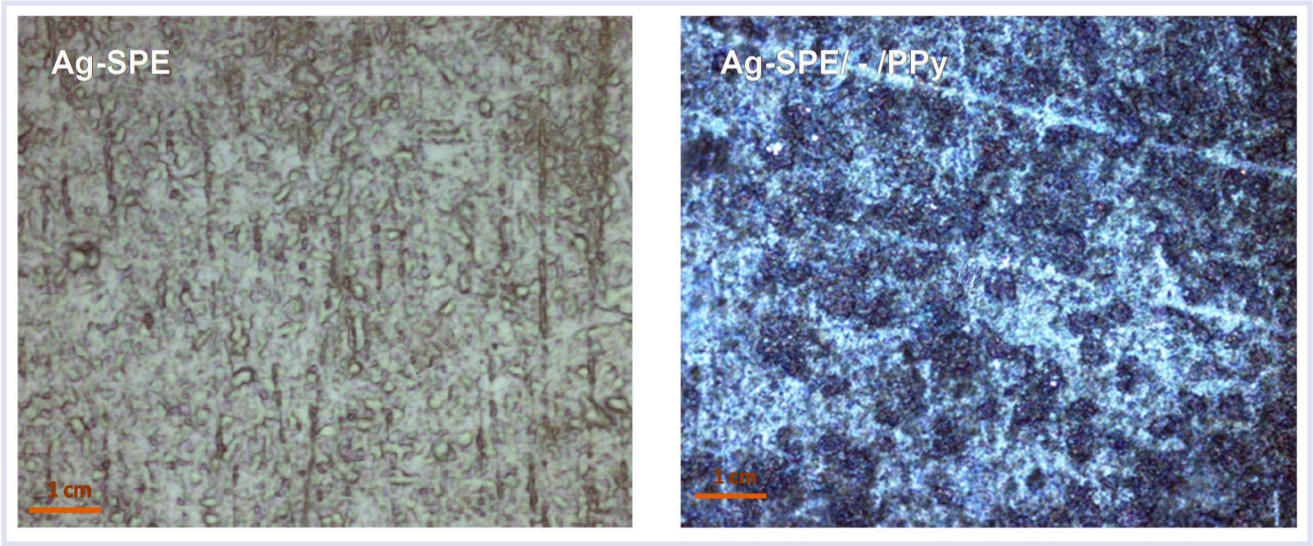

Figure 1.
Confocal microscope analysis (50×) of Ag-SPE and Ag-SPE/—/PPy surfaces.

Europe PMC Funders Author Manuscripts

Europe PMC Funders Author Manuscripts

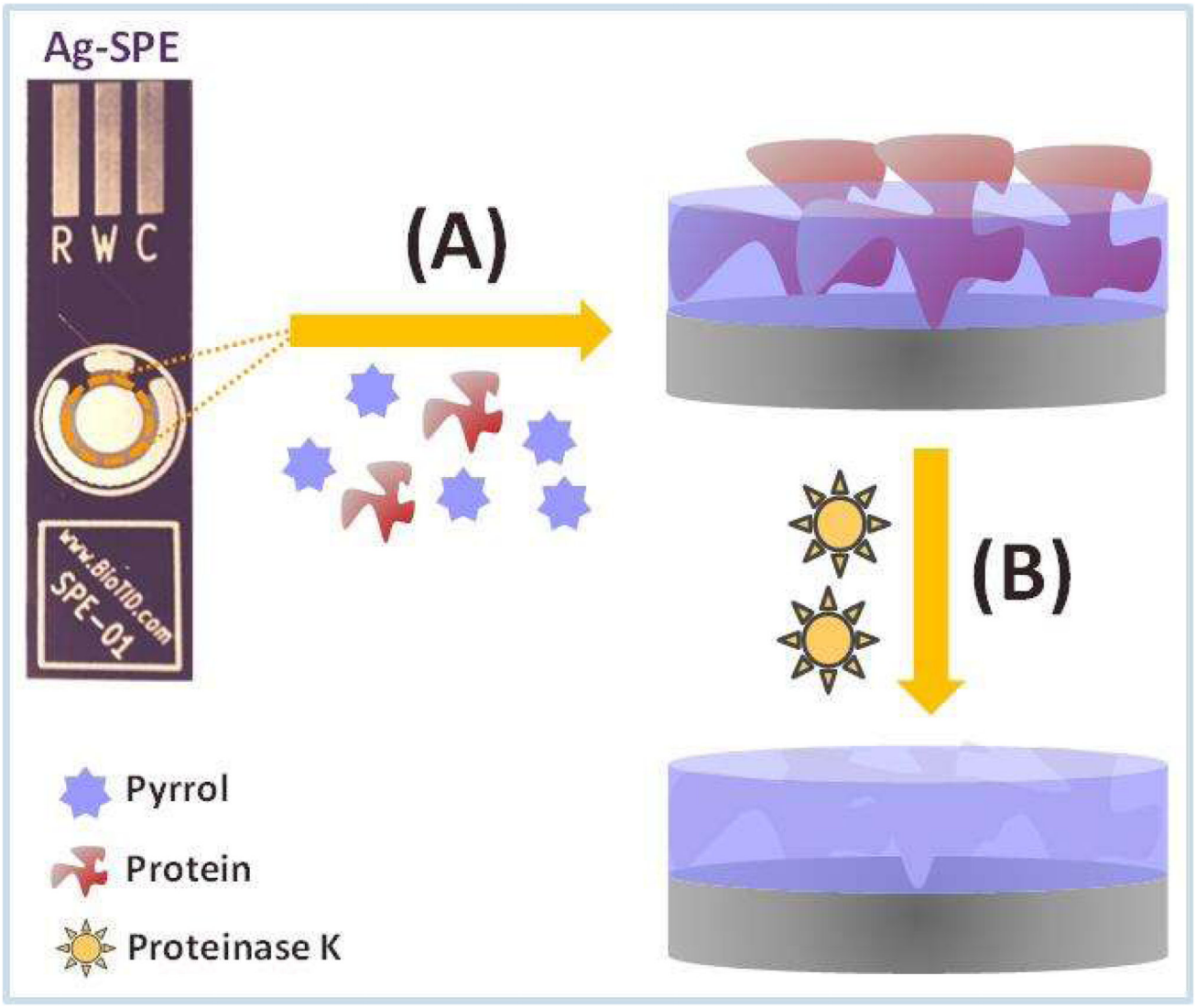

Figure 2.

Schematic representation of the two stages used in the synthesis of Ag-SPE/—/PPy devices. A: electropolymerization of Py in the presence of CEA; B: protein removal by proteinase K.

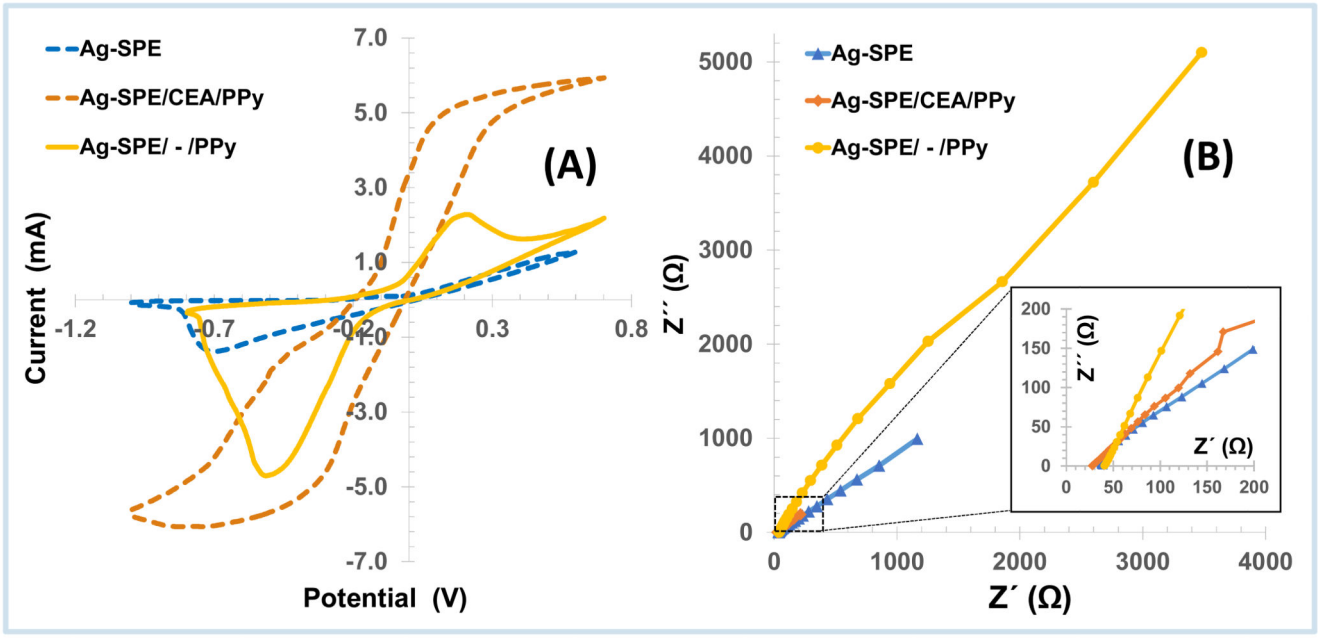

Figure 3.

Electrochemical CV (A) and EIS (B) responses of the different stages of Ag/SPE modification, evaluated in 1.0 mM Ru^{3+}, in buffer, pH 7.2.

Europe PMC Funders Author Manuscripts

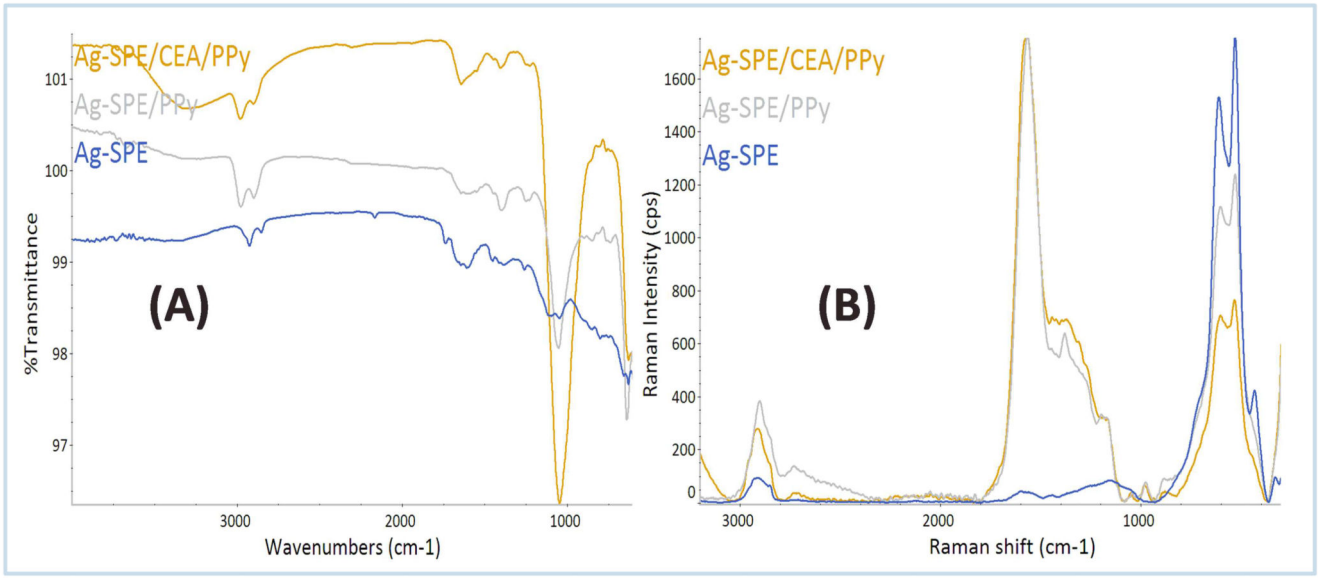

Figure 4.
FTIR (A) and RAMAN (B) spectra corresponding to the direct reading of the working electrode area on Ag-SPE, Ag-SPE/CEA/PPy and Ag-SPE/PPy devices.

Europe PMC Funders Author Manuscripts

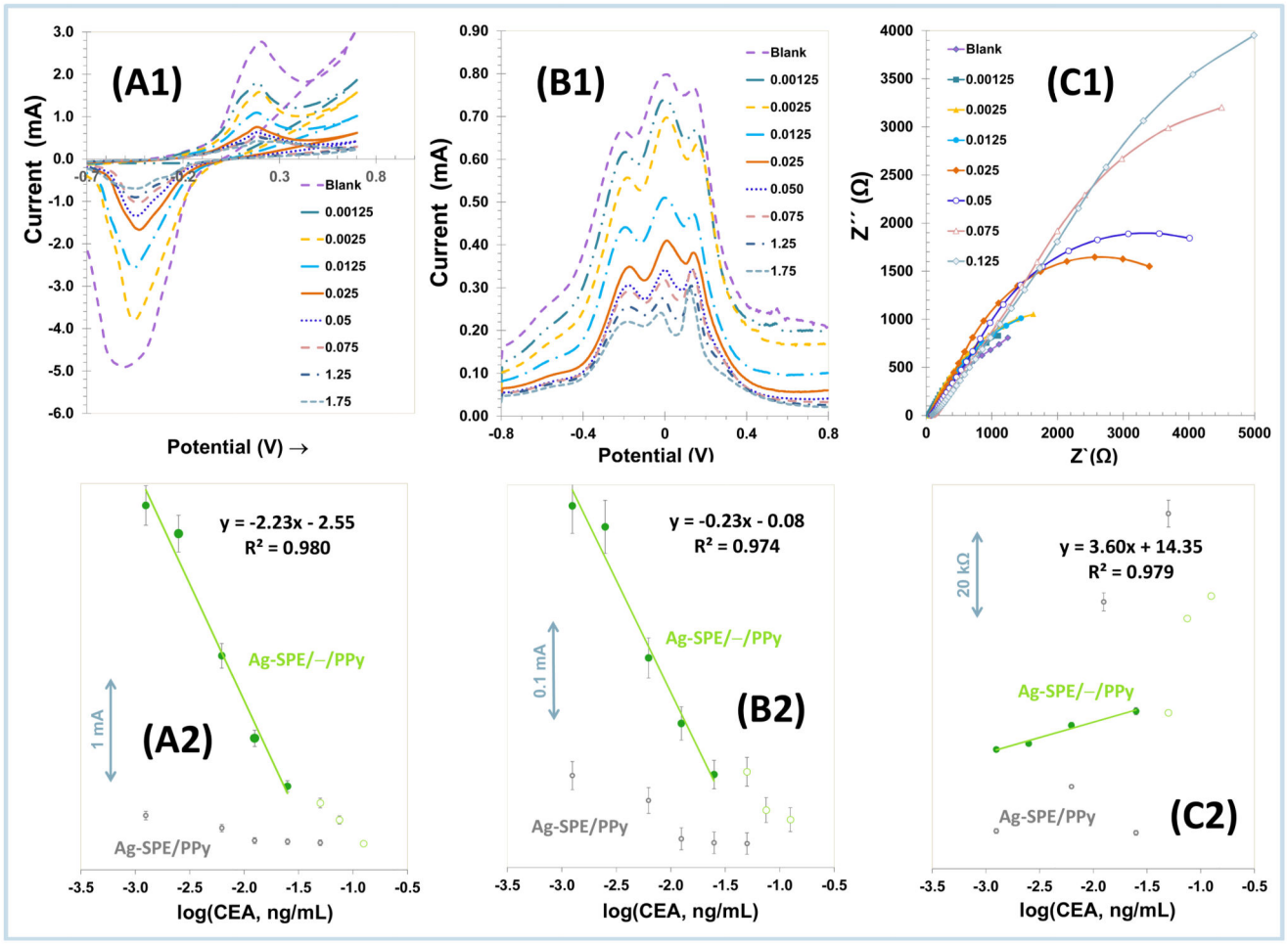

Figure 5.

Electrochemical raw data (1) of Ag-SPE/—/PPy devices in 1.0 mM Ru^{3+}, in buffer, pH 7.2, by CV (A), SWV (B) and EIS (C) readings, after incubation in increasing concentrations of CEA, along with the corresponding calibration curves (2), including also the response of Ag-SPE/PPy for comparison purposes.

Europe PMC Funders Author Manuscripts

Europe PMC Funders Author Manuscripts

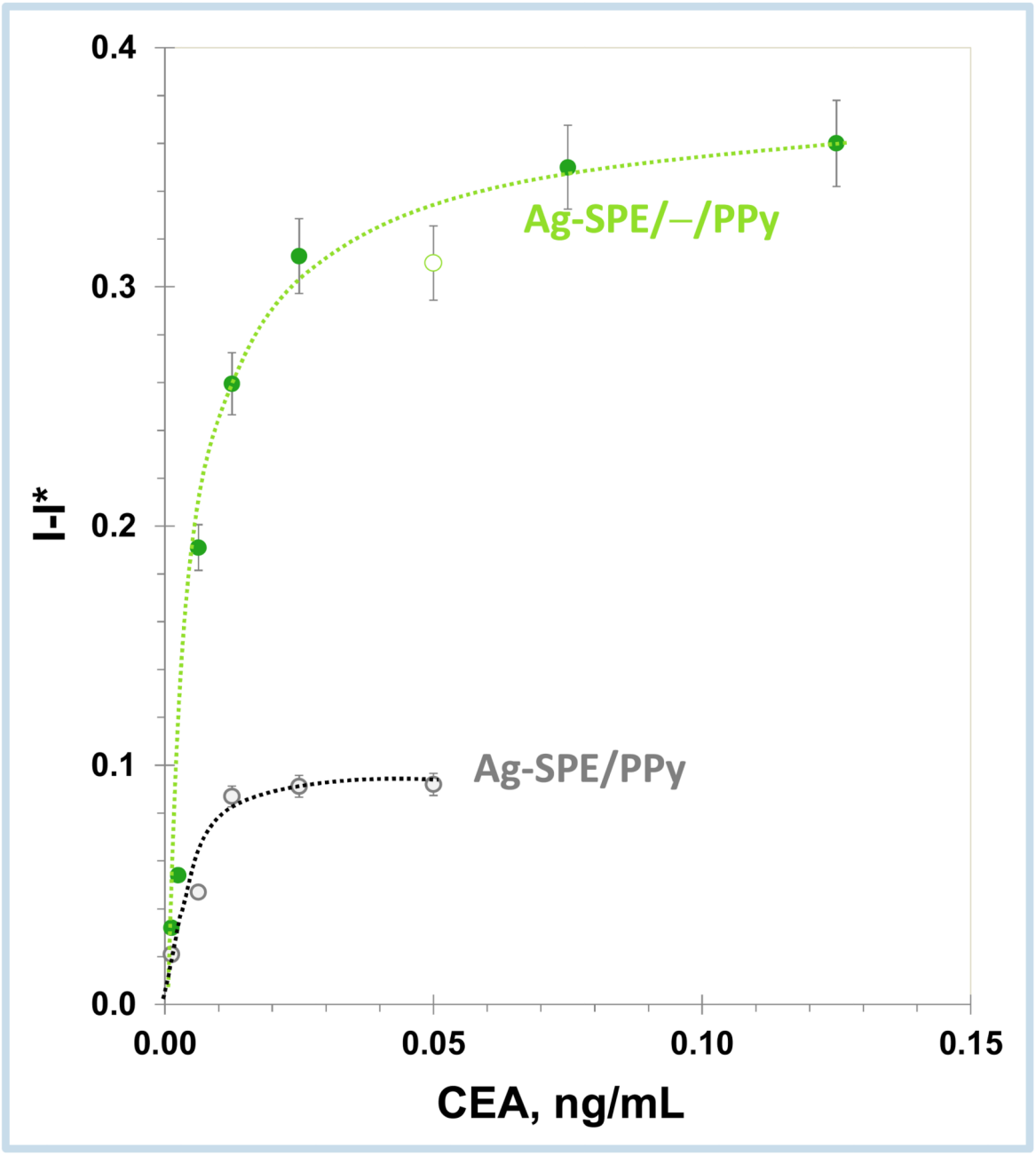

Figure 6.
Graphical representation of the Langmuir isotherm plot for Ag-SPE/—/PPy and Ag-SPE/PPy materials.

Europe PMC Funders Author Manuscripts

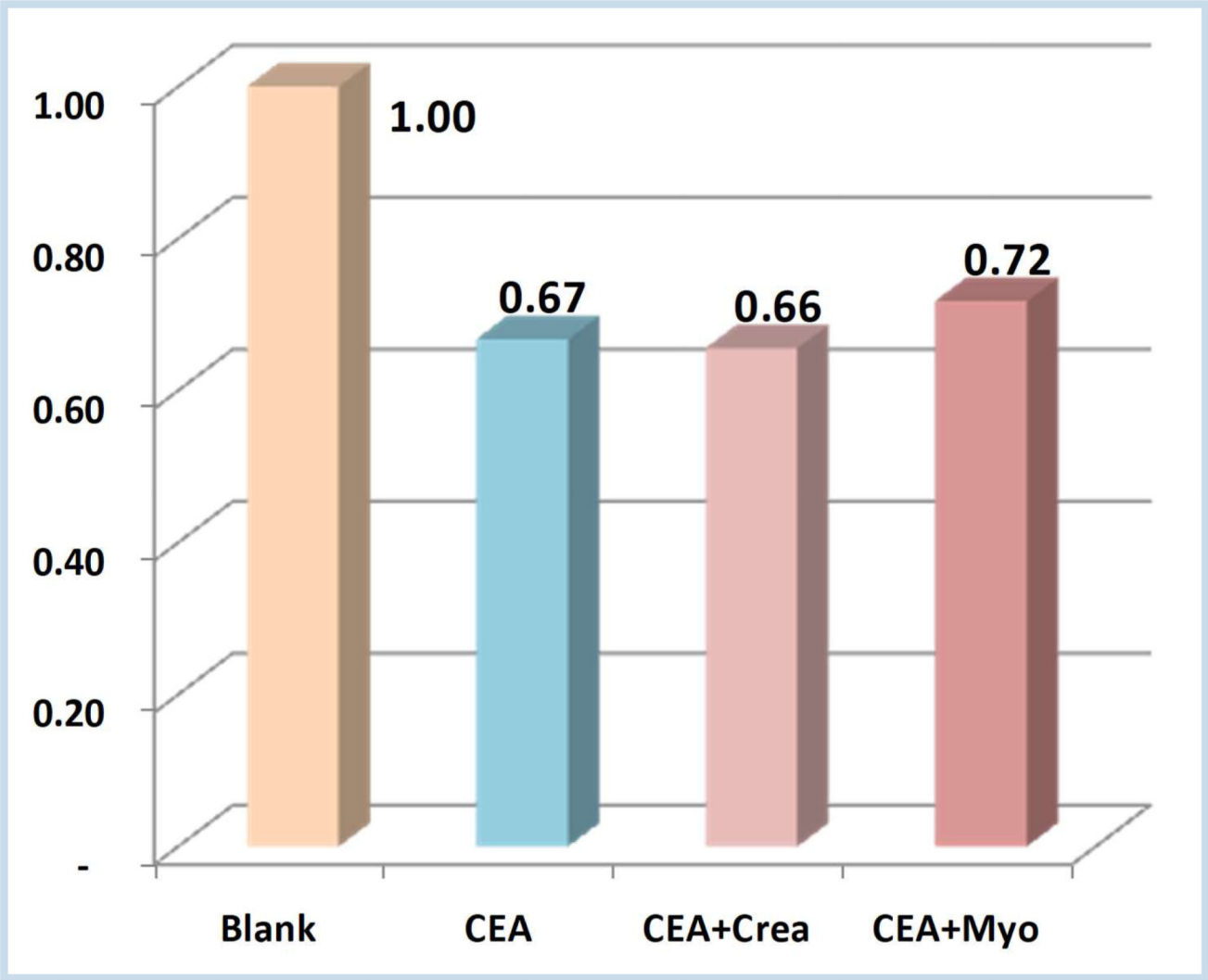

Figure 7.
Selectivity study of the Ag-SPE/—/PPy sensor.